Applied Physics Letters

RESEARCH ARTICLE | SEPTEMBER 19 2023

Compositional dependence of spintronic properties in Pt/GdCo films

Daniel H. Suzuki ; Byung Hun Lee ; Geoffrey S. D. Beach

Appl. Phys. Lett. 123, 122401 (2023)
https://doi.org/10.1063/5.0165884

AIP Publishing

Applied Physics Letters ARTICLE pubs.aip.org/aip/apl

Compositional dependence of spintronic properties in Pt/GdCo films

Cite as: Appl. Phys. Lett. **123**, 122401 (2023); doi: 10.1063/5.0165884
Submitted: 30 June 2023 · Accepted: 26 August 2023 ·
Published Online: 19 September 2023

Daniel H. Suzuki, Byung Hun Lee, and Geoffrey S. D. Beach[a)]

AFFILIATIONS

Department of Materials Science and Engineering, Massachusetts Institute of Technology, Cambridge, Massachusetts 02139, USA

Note: This paper is part of the APL Special Collection on Ferrimagnetic Spintronics.
[a)]**Author to whom correspondence should be addressed:** gbeach@mit.edu

ABSTRACT

GdCo films have been widely used in spintronic applications, owing largely to their tunable degree of ferrimagnetic compensation. However, all key properties likewise depend on the alloy composition, and a systematic study of the interdependent spintronic properties with composition has not been reported. Here, we report the compositional dependence of key spintronic properties, including anisotropy, symmetric, and antisymmetric (Dzyaloshinskii–Moriya, DMI) exchange interactions, effective spin Hall angle, and domain wall mobility in a 3 nm Pt/GdCo composition series. We measure the magnetic anisotropy and determine an interfacial Pt/Co and bulk GdCo pair-ordering contribution to total anisotropy. Additionally, we estimate the exchange stiffness of all three interactions in GdCo as a function of composition. We conduct two types of domain wall motion experiments on patterned racetracks to determine the effective spin Hall angle and current-driven domain wall mobility. We find a 5× increase in effective spin Hall angle with increasing Gd concentration, suggesting an improvement in spin transfer efficiency in rare earth materials. Finally, we observe a monotonic decrease in the DMI strength with increasing Gd content, suggesting that DMI arises from the Pt/Co interfacial interaction.

Rare-earth (RE) transition-metal (TM) amorphous alloys are a promising class of ferrimagnetic materials for spintronics. RE-TM alloys consist of a RE sublattice antiferromagnetically coupled to the TM sublattice. Altering the proportion of RE and TM atoms allows one to control the magnetic properties of RE-TM films, including the saturation magnetization, M_s, net spin density, coercivity, and magnetic anisotropy. This tunability has been used to engineer RE-TM films with low M_s or low net angular momentum, in order to exhibit spintronic phenomena such ultra-small room temperature stable skyrmions,[1,2] high-speed current-driven domain wall motion,[2–5] and voltage-controlled skyrmion generation.[6] However, despite the large volume of work performed on RE-TM films, a comprehensive study of the spintronic properties of RE-TM alloys, particularly in technologically relevant thin films, has yet to be conducted.

In this Letter, we analyze the magnetic properties of 3 nm GdCo across a wide range of compositions with the ultimate aim of quantifying the strength of the Dzyaloshinskii–Moriya interaction (DMI) as a function of composition using 1D domain wall (DW) motion experiments in patterned magnetic racetracks. DMI is an antisymmetric exchange interaction that stabilizes chiral spin textures, a necessity for skyrmion stability and current-driven DW motion. However, extracting this parameter from DW dynamics measurements requires knowledge of other parameters, such as DW width, which depend on material parameters that vary significantly with composition. Here, we undertake a systematic study to quantify all key parameters, providing a roadmap for compositional engineering of skyrmion host materials including magnetic anisotropy and exchange stiffness.

Films of Ta(4)/Pt(4)/Gd_xCo_{1-x}(3)/Ta(4)/Pt(2) were grown by D.C. magnetron sputter deposition (numbers in parenthesis indicate nominal thickness in nanometers) under a background pressure $<2 \times 10^{-7}$ Torr on thermally oxidized Si wafers with $0 \leq x \leq 0.7$. The GdCo layer was grown by co-sputtering from Gd and Co targets with deposition rates of ∼3.5 and ∼1 nm/min, respectively, and with target power densities ranging from 0 to 8.8 and 4.9 W/cm^2, respectively. The lower Pt layer was selected to induce interfacial DMI and inject spin in the adjacent GdCo layer, enabling current-driven DW motion. A thin GdCo layer was chosen to maximize the interfacial DMI while minimizing potential bulk DMI contributions, as have been previously reported in thick RE-TM films.[7] The Ta/Pt cap was

used to prevent sample oxidation while preserving an asymmetric heterostructure for DMI maximization.

The 3 nm GdCo composition series saturation magnetizations, M_s, are shown in Fig. 1(a). Magnetic compensation occurs at $x \approx 0.52$, in contrast to the commonly reported bulk compensation composition of $x \approx 0.22$.[8,9] We have previously explained this discrepancy in terms of a combined environment and dead layer model, in which a RE dead layer results in a reduced average magnetic moment per RE atom (RE atomic magnetic moment) in RE-TM films <10 nm relative to thick films, and the average atomic magnetic moments of both the RE and TM decrease with increasing RE concentration at room temperature.[10] In this model, the thickness of the RE dead layer is independent of RE-TM film thickness and increases with RE concentration, leading to expected Gd dead layer thicknesses of 0.5–2 nm for $x = 0.1 \rightarrow 0.7$ [see Fig. 4(d) of Suzuki *et al.*[10]]. Additionally, at room temperature, the two dominant exchange interactions in RE-TM films are the RE-TM and TM-TM interactions. This results in Gd and Co atomic magnetic moments that depend on the number of Co nearest neighbors, which decreases with increasing x. Thus, at room temperature, the Gd and Co atomic magnetic moments decrease monotonically with increasing x, approaching zero for pure Gd. The combined environment and dead layer model allows for the accurate estimation of individual sublattice contributions, M_{Gd} and M_{Co} (where $M_s = |M_{Gd} - M_{Co}|$), in the grown series, shown as red and blue dashed lines in Fig. 1(a).

Figure 1(b) shows the effective magnetic anisotropy, $K_{u,eff}$, of the GdCo series, measured using hard-axis hysteresis loops via vibrating sample (VSM) and magneto-optical Kerr effect (MOKE) magnetometry. The films exhibit perpendicular magnetic anisotropy (PMA) for compositions $0.27 \lesssim x \lesssim 0.60$. Subtracting the magnetostatic component gives the uniaxial anisotropy constant $K_u = K_{u,eff} + \frac{1}{2}\mu_0 M_s^2$. K_u decreases significantly with increasing Gd concentration at low x and then increases and plateaus from $x = 0.25 \rightarrow 0.45$ before finally tending toward zero for $x > 0.5$. The variation of K_u with x suggests two primary contributions. The most significant contribution is from the Pt/Co interfacial interaction, which is known to promote PMA in ultrathin Pt/Co films, overcoming the large magnetostatic penalty of the Co layer.[11–14] In GdCo, this interaction appears to drop rapidly with increasing Gd content. In addition, anisotropic pair–pair correlations have been found to introduce bulk PMA in RE-TM ferrimagnets.[15–19] This bulk PMA term increases with the number of RE-TM pairs, with pair models indicating a maximum in the pair-ordering induced anisotropy from $0.3 < x < 0.5$, consistent with the observed K_u trend in Fig. 1(b).

Before examining the DW dynamics, we consider the dependence of the exchange stiffness A with composition, which is necessary to predict the DW width $\Delta = \sqrt{A/K_{u,eff}}$ that plays a key role in the dynamical equations of motion. Symmetric exchange in GdCo arises from inter- and intra-sublattice contributions: two ferromagnetic interactions (Gd–Gd and Co–Co) and an antiferromagnetic Gd–Co interaction, $A_{tot} = A_{Gd-Gd} + A_{Co-Co} + A_{Gd-Co}$. The exchange stiffness of each interaction is given by[20,21]

$$A_{ii} = \frac{1}{6} N_a S_i^2 J_{ii} N_c r_{ii}^2 x_i^2, \; A_{ij} = \frac{1}{3} N_a S_i S_j J_{ij} N_c r_{ij}^2 x_i x_j, \tag{1}$$

$$N_a = \frac{0.95}{x v_{Gd} + (1-x) v_{Co}}, \tag{2}$$

with S_i the atomic spin, J_{ij} the exchange energy, x_i the atomic fraction, $N_c = 12$ the coordination number, r_{ij} the interatomic spacing ($r_{Gd-Gd} = 3.58 \times 10^{-10}$ m, $r_{Gd-Co} = 3.02 \times 10^{-10}$ m, $r_{Co-Co} = 2.50 \times 10^{-10}$ m),[20] and N_a the number of atoms per unit volume, assuming that the density of the amorphous film is 95% of its crystalline counterpart as has been reported previously.[21–23] The atomic volumes were taken to be $v_{Gd} = 3.305 \times 10^{-29}\,\mathrm{m}^3$ and $v_{Co} = 1.100 \times 10^{-29}\,\mathrm{m}^3$, derived from their bulk densities. Thick film GdCo J_{ij} values from Hansen *et al.*[9] and Gangulee and Kobliska[20] were used for calculations [Fig. 2(a)]. Both J_{Gd-Gd} and J_{Gd-Co} are independent of composition; however, J_{Co-Co} decreases linearly with increasing Gd concentration. Additionally, in GdCo thin films, the Gd dead layer results in an alloyed composition that is Gd poor compared to its nominal composition. The true alloyed composition $\tilde{x}$ can be estimated from the nominal composition x using the relations[10]

$$\tilde{x} = \frac{(t - t_{Gd}) x v_{Gd} - t_{Gd}(1-x) v_{Co}}{(t - t_{Gd} x) v_{Gd} - t_{Gd}(1-x) v_{Co}}, \tag{3}$$

$$t_{Gd}(x) = \frac{x v_{Gd}}{x v_{Gd} + (1-x) v_{Co}} t_{Gd,\max}, \tag{4}$$

with $t = 3$ nm the nominal film thickness and $t_{Gd,\max} = 2.22$ nm the maximum Gd dead layer thickness determined previously.[10] Assuming J_{Co-Co} is dependent on $\tilde{x}$, Eq. (3) is used to determine J_{Co-Co} at nominal composition x. To determine the S_i, we utilize the combined environment and dead layer model referenced previously,

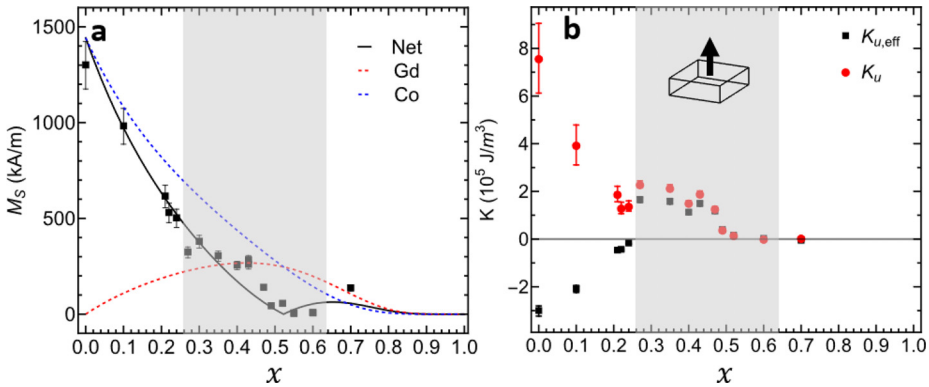

FIG. 1. Magnetic properties of 3 nm Gd_xCo_{1-x} films. (a) Saturation magnetization, M_s, as a function of composition. The solid black line is the combined environment and dead layer model fit.[10] The red and blue dashed lines are expected Gd and Co sublattice contributions predicted by the model (M_{Gd} and M_{Co}), respectively. (b) Effective anisotropy energy density (black squares), $K_{u,eff}$, and uniaxial energy density (red circles), K_u, as a function of composition. The shaded region in (a) and (b) indicates perpendicular magnetic anisotropy.

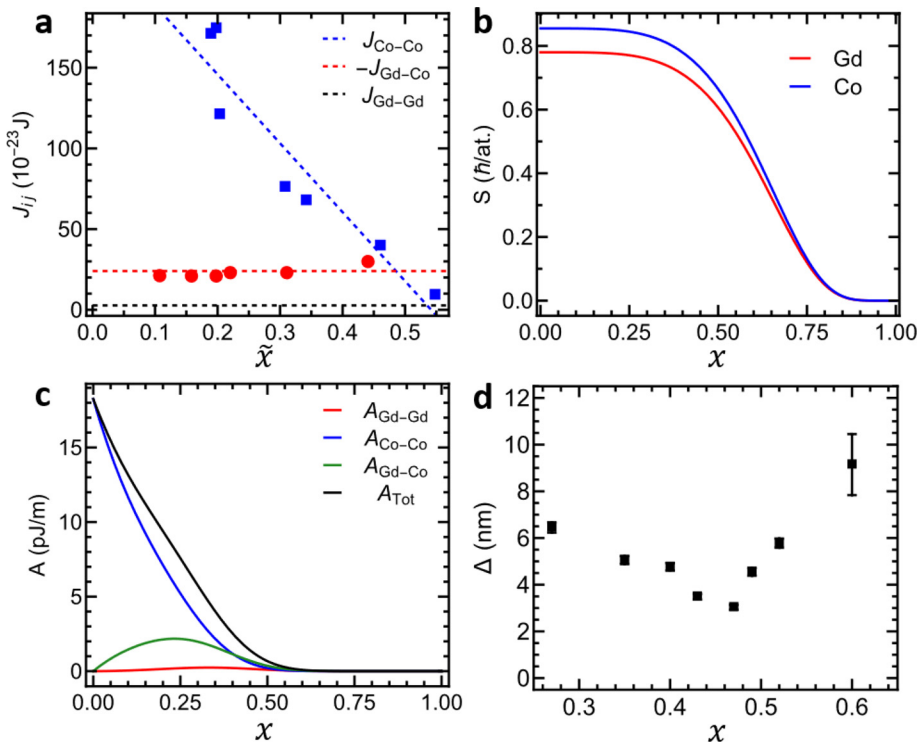

FIG. 2. Symmetric exchange in GdCo films. (a) Previously reported exchange energy values in thick GdCo films as a function of alloyed Gd composition, $\tilde{x}$ (see the text). Red and blue data points are from Hansen.[9] The black dotted line is from Gangulee.[20] (b) Expected average atomic spin of Gd and Co in 3 nm GdCo as a function of nominal composition, x. (c) Calculated 3 nm GdCo exchange stiffness, separated by each interaction. (d) Calculated domain wall width, Δ, of 3 nm GdCo samples exhibiting PMA.

which predicts the average atomic spin for each species in 3 nm GdCo [Fig. 2(b)]. The Gd spin value is reduced from its standard bulk value of $3.5\,\hbar/at$ due to dilution with a non-magnetic Gd dead layer at room temperature and monotonically decreases with increasing x due to decreased Co nearest neighbors.

Combining J_{ij} and S_i yields the exchange stiffness of each interaction in GdCo, shown in Fig. 2(c). As expected, due to the low Curie temperature of Gd ($T_{c,Gd} \approx 290$ K), A_{Gd-Gd} is insignificant compared to the other two interactions at room temperature. Additionally, the Co–Co interaction dominates except at relatively high $x > 0.4$. The value of A_{tot} is reduced by an order of magnitude from $x = 0 \rightarrow 0.5$ as the Co–Co exchange is reduced due to fewer Co–Co pairs. We have estimated $\Delta = \sqrt{A_{tot}/K_{u,eff}}$ using the sum of the inter- and intra-sublattice exchange stiffness, as shown in Fig. 2(d). Despite the large decrease in exchange stiffness over this range, the corresponding reduction in anisotropy results in a relatively weak variation of Δ, ranging from ∼3 to 9 nm in the studied range.

GdCo PMA samples with $x = 0.27 \rightarrow 0.49$ were patterned into $40 \times 100\ \mu m^2$ magnetic racetracks for DW motion experiments [Fig. 3(a)]. Kerr microscopy was used to observe DW displacement. Two types of experiments were conducted: depinning and velocity measurements. In the depinning experiment, a low DC density, $j\,(\sim 10^9\ A/m^2)$, was applied along the length of the track and an assisting out-of-plane (OOP) magnetic field was slowly ramped from zero until a critical field, H_{dp}, was reached and the propagated freely along a length of the track of at least ∼30 μm. With no applied longitudinal field, H_x, both up–down and down–up DWs exhibit the same linear relationship between j and H_{dp}, consistent with previous observations [Fig. 3(b)].[2,24] The slope of Fig. 3(b) gives the spin–orbit torque (SOT) effective field per unit current density, χ, the proportionality constant between current density j and spin Hall effective field, $H_{SH} = \chi j$. Figure 3(c) shows χ as a function of composition. χ is found to exponentially increase with decreasing M_s [see Fig. 1(a)], consistent with previous reports near magnetic compensation.[25–27] To separate the compositional dependence of χ from its M_s dependence, the effective spin-Hall angle was calculated using[28]

$$\theta_{SH}^{eff} = \frac{4e\mu_0 M_s t}{\pi\hbar}\chi, \tag{5}$$

where e is elementary charge. θ_{SH}^{eff} is found to increase with increasing x [Fig. 3(d)]. A similar increase in θ_{SH}^{eff} in TbCo with increasing Tb content was reported in Ref. 29, and theoretical work has shown significant SOT generated by RE atoms, particularly when alloyed.[30] The determination of θ_{SH}^{eff} here relies on DW depinning measurements that observe net SOT phenomena. As a result, the extracted θ_{SH}^{eff} does not distinguish between individual sublattices (that is, Pt/Co vs Pt/Gd interaction); only the combined effect is measured. The increase in θ_{SH}^{eff} with RE content suggests that the RE sublattice enhances spin transmission in RE-TM alloys.

We next examine DW velocity v as a function of j and H_x. DW displacement was measured by Kerr microscopy. Current pulses of 5 ns were used to drive DW motion. In magnetic racetracks, the DMI stabilizes homochiral Néel DWs via an effective field, H_D, perpendicular to the wall. The homochiral Néel walls enable translational current-induced DW motion. The DW velocity, v, in ferrimagnetic materials is well-described by the 1D model:[31]

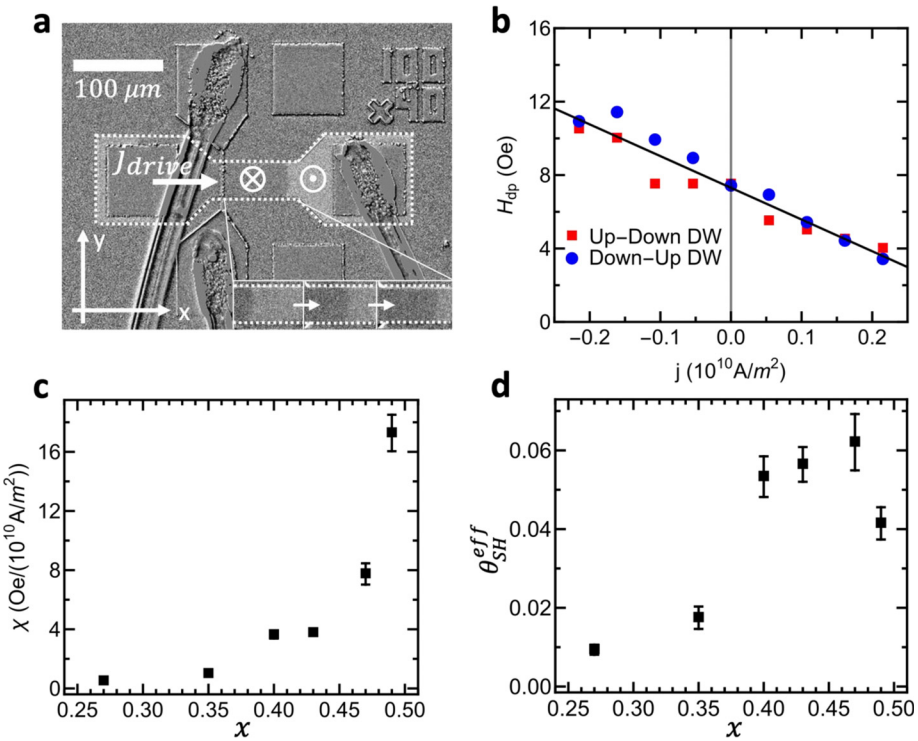

FIG. 3. Domain wall depinning experiments. (a) Image of magnetic racetrack device used for de-pinning and DW velocity experiments showing a down-up DW. Inset, series of images showing DW displacement in $Gd_{0.47}Co_{0.53}$ with $j_{drive} = +11.5 \times 10^{11}$ A/m^2 and a train of 5 ns current pulses totaling 100 ns between images. (b) Exemplary plot of depinning field, H_{dp}, vs applied DC drive current, j, in $Gd_{0.49}Co_{0.51}$. (c) SOT effective field per unit current density of 3 nm GdCo films as a function of composition. (d) Effective spin-Hall angle as a function of composition.

$$v = \frac{\frac{\pi}{2}\gamma_{eff}\Delta\,\mu_0 H_{SH}}{\sqrt{\alpha_{eff}^2 + \left(\frac{H_{SH}}{H_D+H_x}\right)^2}}, \tag{6}$$

where γ_{eff} is the effective gyromagnetic ratio and α_{eff} is the effective Gilbert damping, ferrimagnetic analogues of the ferromagnetic magnetic properties.[2,32] v was first measured under $H_x = 0$ and varying j [Figs. 4(a)–4(c)]. v initially increases linearly with j before saturating at an asymptotic velocity, $v_{\max} \approx \frac{\pi}{2}\gamma_{eff}\Delta\,\mu_0(H_D + H_x)$. In the saturation regime, v varies linearly with H_x, and extrapolation to zero yields H_D. However, the saturation current density, j_{sat}, which we define here as the current density required to reach 90% of $v_{\max}$ with $H_x = 0$, is composition dependent. This is evidenced by comparison of Figs. 4(a) and 4(b), in which v approaches saturation at $j_{sat} \approx 16 \times 10^{11}$ A/m^2 and $j_{sat} > 20 \times 10^{11}$ A/m^2, respectively. Figures 4(d)–4(f) show measurements of v vs H_x at three representative compositions. The DMI-stabilized homochiral DWs result in H_D with opposite signs for up–down and down–up DWs. As a consequence, up-down and down-up DWs have inverse responses to H_x, i.e., larger H_x decreases $v_{up-down}$ but increases $v_{down-up}$ [Figs. 4(d)–4(f)]. The consistent sign of H_D for each type of DW across $x = 0.27 \rightarrow 0.49$ indicates no chirality change (or equivalently sign flip in D) across this composition range. As j decreases below j_{sat}, the v vs H_x data become increasingly nonlinear [Fig. 4(e)]. A linear fit assuming saturation behavior would result in a large overestimation of H_D. To properly account for the curvature of v vs H_x at $v < v_{\max}$, the data in Figs. 4(a)–4(c) and Figs. 4(d)–4(f) were fitted to the full 1D model [Eq. (6)]. The χ of each sample determined from the previous depinning experiments [Fig. 3(c)] was used to convert the applied current density to a spin-Hall effective field. The fits of the 1D model are shown as solid lines in Fig. 4.

The combined results of the DW motion experiments are shown in Fig. 5. Both α_{eff} and g_{eff} [Figs. 5(a) and 5(d)] show divergent behavior near $x \approx 0.42$, suggesting that the angular momentum compensation composition of 3 nm GdCo is near that point. We observe >10× higher α_{eff} on the Gd-dominated side of angular momentum compensation compared the Co-dominated side. We attribute this significant increase in α_{eff} to the presence of the Gd dead layer potentially increasing surface roughness, which has been shown to enhance damping.[33] α_{eff} and γ_{eff} are combined to determine the DW mobility μ,

$$\mu = \frac{\pi\,\gamma_{eff}\Delta}{2\alpha_{eff}} \tag{7}$$

shown in Fig. 5(e). μ decreases exponentially with increasing Gd content, primarily due to the reduction in the DW width, Δ, over this range. The ∼30x reduction in μ from $x = 0.27 \rightarrow 0.49$ is almost equivalent to the increase in χ [Fig. 3(c)] observed over the same range, resulting in near-constant slopes in the v vs j data at all x at small j [Figs. 4(a)–4(c)].

The saturation velocity, v_{max}, at $H_x = 0$ is shown in Fig. 5(b). With no applied longitudinal field, $v_{\max} = \frac{\pi D}{2S}$, with $S = \frac{\hbar M_s}{\mu_B g_{eff}}$ the net spin density. The $v_{\max}$ data exhibit constant $v_{\max} \approx 300$ m/s except near the angular momentum compensation point ($S = 0$), where $v_{\max} \approx 400$ m/s. This is consistent with previous investigations of ferrimagnetic materials near angular momentum compensation where the DW velocity has similarly increased with reduced spin density.[2–4] The $v_{\max}$ data suggest that except at $S \approx 0$, the ratio D/S remains approximately constant.

Finally, the effective DMI field, H_D, was extracted from the v vs H_x data and is presented in Fig. 5(c). The measured H_D ranges from

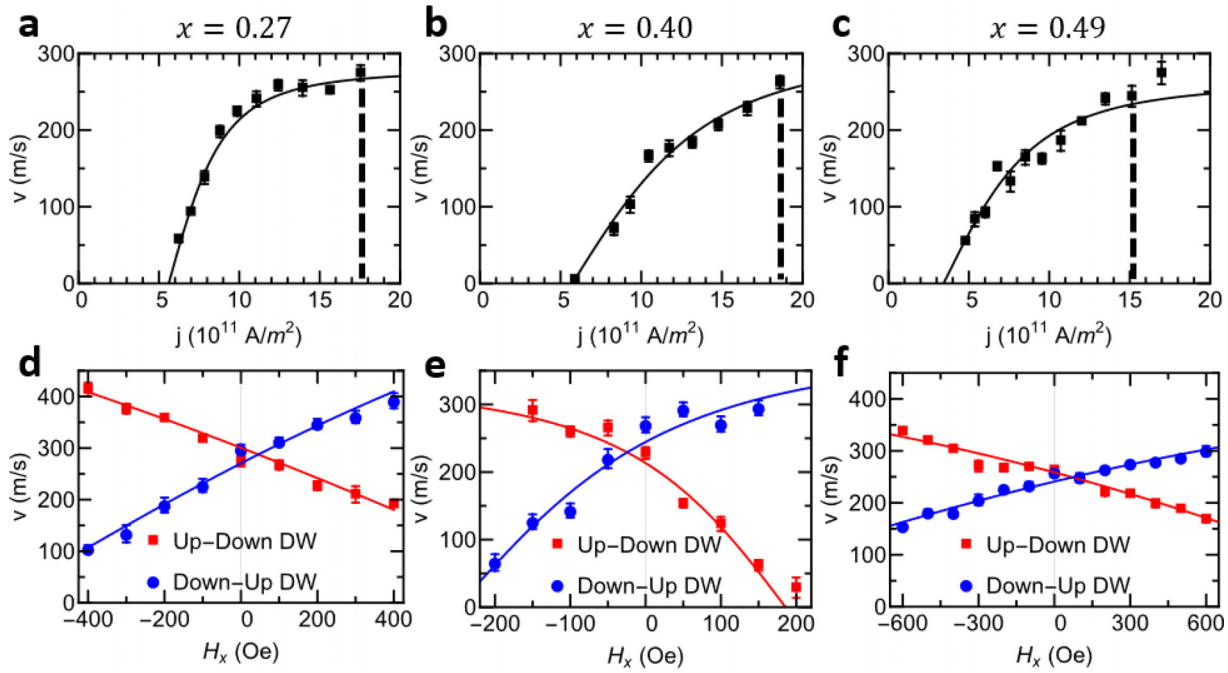

FIG. 4. Current-induced domain wall velocity measurements in Pt/GdCo heterostructures at three representative compositions. (a)–(c) Domain wall velocity, v, vs applied current density, j, with no applied longitudinal field. Dotted line indicates j used for corresponding v vs H_x measurement below. (d)–(f) Domain wall velocity vs applied longitudinal magnetic field, H_x. Solid lines are fits to the 1D model (see the text). The error bars are the standard error of 5–20 measurements.

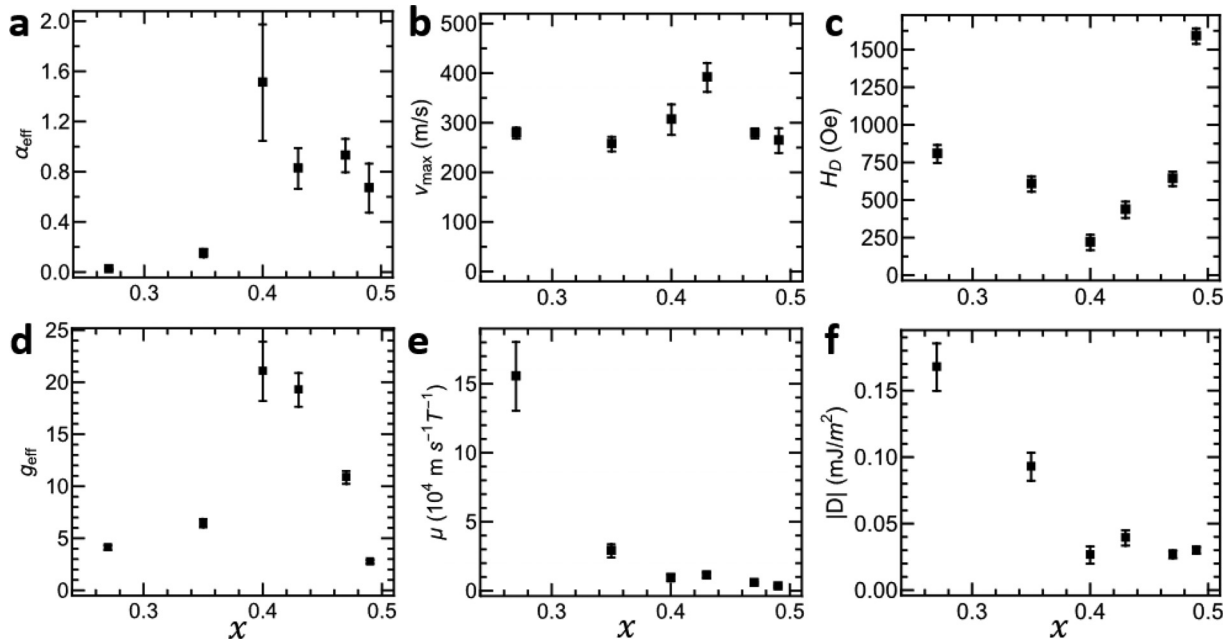

FIG. 5. Pt/Gd_xCo_{1-x} dynamic properties as a function of composition. (a) Effective damping. (b) Maximum domain wall velocity. (c) DMI effective field. (d) Effective g-factor. (e) Domain wall mobility. (f) DMI magnitude.

250 to ∼1700 Oe with a minimum at $x = 0.4$. There is no clear H_D trend evident as a function of composition. However, H_D depends on M_s and Δ, which both also depend on composition. To isolate the strength of the DMI as a function of Gd composition, H_D was converted to D using[31,34]

$$D = \mu_0 M_s H_D \Delta. \tag{8}$$

The results are plotted in Fig. 5(f), where a clear trend emerges. We observe a monotonic decrease with increasing Gd content across the entire PMA composition range, suggesting that the Pt/Co interaction is primarily responsible for the occurrence of DMI in GdCo films and that the addition of Gd only dilutes the strength of the DMI. The value of D at $x = 0.44$ is smaller than the reported DMI in a 6 nm film at the same composition.[2] At $x = 0.27$, we find a similar value of D compared to a previous report on a 5 nm film.[35] In heavy metal/ferromagnetic systems, $D \propto \frac{1}{t}$ when induced at an interface,[36] making the reduced D values observed in 3 nm GdCo surprising. Composition gradients in RE-TM alloys have been shown to induce a bulk DMI with $D \propto t$.[7] This could add a second contribution to the DMI in films >3 nm that results in larger D values that is insignificant in our thinner films. We note that the measured χ values [Fig. 3(c)] are also lower than the reported SOT in 6 nm GdCo,[2] which, combined with a reduced D, results in lower DW velocities than previously observed. Because DMI is sensitive to interfacial quality,[37–40] we ascribe both of these effects to increased surface roughness in thin GdCo films, potentially due to the significant dead fraction of Gd present in 3 nm films, particularly at high Gd concentrations.

In summary, we have analyzed the spintronic properties of 3 nm GdCo. A number of GdCo magnetic properties critical to spintronic devices and stabilization of chiral spin textures are found to strongly depend on RE concentration. The total effective anisotropy is found to strongly decrease with increased Gd concentration, consistent with a Pt/Co interfacial origin. We also observe a subdominant increase in uniaxial anisotropy that is maximized at $x \approx 0.4$, consistent with a pair-ordering bulk anisotropy origin that is often used to explain bulk PMA in RE-TM alloys. The combination of DW velocity and depinning measurements under longitudinal and polar applied fields allows for determination of a variety of dynamic magnetic properties in Pt/GdCo heterostructures, including DMI effective field, damping, spin density, spin transfer efficiency, and effective spin-Hall angle. These fundamental measurements are combined with knowledge of the ferromagnetic and antiferromagnetic exchange interactions in GdCo to determine the magnitude of antisymmetric exchange constant D. D is found to monotonically decrease with increasing Gd content, suggesting that the Pt/Co interface is the primary source of DMI in Pt/GdCo films. This thorough characterization of GdCo's spintronic properties should allow for improved design of materials for next-generation DW and skyrmionics devices.

This work was supported in part by the DARPA TEE Program and the Samsung Global Research Outreach (GRO) Program.

AUTHOR DECLARATIONS

Conflict of Interest

The authors have no conflicts to disclose.

Author Contributions

Daniel Hiroshi Suzuki: Conceptualization (equal); Data curation (equal); Formal analysis (equal); Investigation (equal); Methodology (equal); Software (equal); Visualization (equal); Writing – original draft (equal); Writing – review & editing (equal). **Byung Hun Lee:** Data curation (supporting); Formal analysis (supporting); Methodology (supporting); Writing – review & editing (supporting). **Geoffrey S. D. Beach:** Conceptualization (equal); Formal analysis (equal); Funding acquisition (equal); Methodology (equal); Project administration (equal); Resources (equal); Supervision (equal); Writing – review & editing (equal).

DATA AVAILABILITY

The data that support the findings of this study are available from the corresponding author upon reasonable request.

REFERENCES

[1] F. Büttner, I. Lemesh, M. Schneider, B. Pfau, C. M. Günther, P. Hessing, J. Geilhufe, L. Caretta, D. Engel, B. Krüger, J. Viefhaus, S. Eisebitt, and G. S. D. Beach, "Field-free deterministic ultrafast creation of magnetic skyrmions by spin-orbit torques," Nat. Nanotechnol. **12**(11), 1040–1044 (2017).
[2] L. Caretta, M. Mann, F. Büttner, K. Ueda, B. Pfau, C. M. Günther, P. Hessing, A. Churikova, C. Klose, M. Schneider, D. Engel, C. Marcus, D. Bono, K. Bagschik, S. Eisebitt, and G. S. D. Beach, "Fast current-driven domain walls and small skyrmions in a compensated ferrimagnet," Nat. Nanotechnol. **13**(12), 1154–1160 (2018).
[3] M. Binder, A. Weber, O. Mosendz, G. Woltersdorf, M. Izquierdo, I. Neudecker, J. R. Dahn, T. D. Hatchard, J.-U. Thiele, C. H. Back, and M. R. Scheinfein, "Magnetization dynamics of the ferrimagnet CoGd near the compensation of magnetization and angular momentum," Phys. Rev. B **74**(13), 134404 (2006).
[4] K.-J. Kim, S. K. Kim, Y. Hirata, S.-H. Oh, T. Tono, D.-H. Kim, T. Okuno, W. S. Ham, S. Kim, G. Go, Y. Tserkovnyak, A. Tsukamoto, T. Moriyama, K.-J. Lee, and T. Ono, "Fast domain wall motion in the vicinity of the angular momentum compensation temperature of ferrimagnets," Nat. Mater. **16**(12), 1187–1192 (2017).
[5] C. D. Stanciu, A. V. Kimel, F. Hansteen, A. Tsukamoto, A. Itoh, A. Kirilyuk, and T. Rasing, "Ultrafast spin dynamics across compensation points in ferrimagnetic GdFeCo: The role of angular momentum compensation," Phys. Rev. B **73**(22), 220402 (2006).
[6] M. Huang, M. U. Hasan, K. Klyukin, D. Zhang, D. Lyu, P. Gargiani, M. Valvidares, S. Sheffels, A. Churikova, F. Büttner, J. Zehner, L. Caretta, K. Y. Lee, J. Chang, J. P. Wang, K. Leistner, B. Yildiz, and G. S. D. Beach, "Voltage control of ferrimagnetic order and voltage-assisted writing of ferrimagnetic spin textures," Nat. Nanotechnol. **16**(9), 981–988 (2021).
[7] D.-H. Kim, M. Haruta, H.-W. Ko, G. Go, H.-J. Park, T. Nishimura, D.-Y. Kim, T. Okuno, Y. Hirata, Y. Futakawa, H. Yoshikawa, W. Ham, S. Kim, H. Kurata, A. Tsukamoto, Y. Shiota, T. Moriyama, S.-B. Choe, K.-J. Lee, and T. Ono, "Bulk Dzyaloshinskii–Moriya interaction in amorphous ferrimagnetic alloys," Nat. Mater. **18**(7), 685–690 (2019).
[8] P. Hansen and H. Heitmann, "Media for erasable magnetooptic recording," IEEE Trans. Magn. **25**(6), 4390–4404 (1989).
[9] P. Hansen, C. Clausen, G. Much, M. Rosenkranz, and K. Witter, "Magnetic and magneto-optical properties of rare-earth transition-metal alloys containing Gd, Tb, Fe, Co," J. Appl. Phys. **66**(2), 756–767 (1989).
[10] D. H. Suzuki, M. Valvidares, P. Gargiani, M. Huang, A. E. Kossak, and G. S. D. Beach, "Thickness and composition effects on atomic moments and magnetic compensation point in rare-earth transition-metal thin films," Phys. Rev. B **107**(13), 134430 (2023).
[11] C.-F. Pai, Y. Ou, L. H. Vilela-Leão, D. C. Ralph, and R. A. Buhrman, "Dependence of the efficiency of spin Hall torque on the transparency of Pt/ferromagnetic layer interfaces," Phys. Rev. B **92**(6), 064426 (2015).

[12]W. Y. Kim, H. K. Gweon, K. J. Lee, and C. Y. You, "Correlation between interfacial Dzyaloshinskii-Moriya interaction and interfacial magnetic anisotropy of Pt/Co/MgO structures," Appl. Phys. Express **12**(5), 053007 (2019).
[13]P. F. Carcia, "Perpendicular magnetic anisotropy in Pd/Co and Pt/Co thin-film layered structures," J. Appl. Phys. **63**(10), 5066–5073 (1988).
[14]M. Belmeguenai, J.-P. Adam, Y. Roussigné, S. Eimer, T. Devolder, J. Kim, S. M. Cherif, A. Stashkevich, and A. Thiaville, "Interfacial Dzyaloshinskii-Moriya interaction in perpendicularly magnetized Pt/Co/AlO_x ultrathin films measured by Brillouin light spectroscopy," Phys. Rev. B **91**, 180405 (2015).
[15]K. Ueda, A. J. Tan, and G. S. D. Beach, "Effect of annealing on magnetic properties in ferrimagnetic GdCo alloy films with bulk perpendicular magnetic anisotropy," AIP Adv. **8**(12), 125204 (2018).
[16]V. G. Harris, W. T. Elam, N. C. Koon, and F. Hellman, "Deposition-temperature dependence of structural anisotropy in amorphous Tb-Fe films," Phys. Rev. B **49**(5), 3637–3640 (1994).
[17]R. C. Taylor and A. Gangulee, "Magnetization and magnetic anisotropy in evaporated GdCo amorphous films," J. Appl. Phys. **47**(10), 4666–4668 (1976).
[18]K. Ueda, M. Mann, C.-F. Pai, A.-J. Tan, and G. S. D. Beach, "Spin-orbit torques in Ta/Tb_xCo_{100-x} ferrimagnetic alloy films with bulk perpendicular magnetic anisotropy," Appl. Phys. Lett. **109**(23), 232403 (2016).
[19]J. C. S. Lévy and D. Mercier, "Amorphous structures: A local analysis," J. Appl. Phys. **53**(11), 7709–7712 (1982).
[20]A. Gangulee and R. J. Kobliska, "Magnetic properties of amorphous Co-Gd-Mo-Ar thin films," J. Appl. Phys. **49**(7), 4169–4173 (1978).
[21]A. Gangulee and R. J. Kobliska, "Mean field analysis of the magnetic properties of amorphous transition-metal–rare-earth alloys," J. Appl. Phys. **49**(9), 4896–4901 (1978).
[22]H. S. Chen and B. K. Park, "Role of chemical bonding in metallic glasses," Acta Metall. **21**(4), 395–400 (1973).
[23]G. S. Cargill, "Dense random packing of hard spheres as a structural model for noncrystalline metallic solids," J. Appl. Phys. **41**(5), 2248–2250 (1970).
[24]S. Emori, E. Martinez, K.-J. Lee, H.-W. Lee, U. Bauer, S.-M. Ahn, P. Agrawal, D. C. Bono, and G. S. D. Beach, "Spin Hall torque magnetometry of Dzyaloshinskii domain walls," Phys. Rev. B **90**(18), 184427 (2014).
[25]W. Seung Ham, S. Kim, D.-H. Kim, K.-J. Kim, T. Okuno, H. Yoshikawa, A. Tsukamoto, T. Moriyama, and T. Ono, "Temperature dependence of spin-orbit effective fields in Pt/GdFeCo bilayers," Appl. Phys. Lett. **110**(24), 242405 (2017).
[26]C.-F. Pai, M. Mann, A. J. Tan, and G. S. D. Beach, "Determination of spin torque efficiencies in heterostructures with perpendicular magnetic anisotropy," Phys. Rev. B **93**(14), 144409 (2016).
[27]K. Ueda, M. Mann, P. W. P. P. de Brouwer, D. Bono, and G. S. D. D. Beach, "Temperature dependence of spin-orbit torques across the magnetic compensation point in a ferrimagnetic TbCo alloy film," Phys. Rev. B **96**(6), 64410 (2017).
[28]A. Thiaville, S. Rohart, É. Jué, V. Cros, and A. Fert, "Dynamics of Dzyaloshinskii domain walls in ultrathin magnetic films," EPL (Europhys. Lett.) **100**(5), 57002 (2012).
[29]S.-G. Je, J.-C. Rojas-Sánchez, T. H. Pham, P. Vallobra, G. Malinowski, D. Lacour, T. Fache, M.-C. Cyrille, D.-Y. Kim, S.-B. Choe, M. Belmeguenai, M. Hehn, S. Mangin, G. Gaudin, and O. Boulle, "Spin-orbit torque-induced switching in ferrimagnetic alloys: Experiments and modeling," Appl. Phys. Lett. **112**(6), 062401 (2018).
[30]N. Reynolds, P. Jadaun, J. T. Heron, C. L. Jermain, J. Gibbons, R. Collette, R. A. Buhrman, D. G. Schlom, and D. C. Ralph, "Spin Hall torques generated by rare-earth thin films," Phys. Rev. B **95**(6), 064412 (2017).
[31]E. Martinez, S. Emori, N. Perez, L. Torres, and G. S. D. Beach, "Current-driven dynamics of Dzyaloshinskii domain walls in the presence of in-plane fields: Full micromagnetic and one-dimensional analysis," J. Appl. Phys. **115**(21), 213909 (2014).
[32]R. K. Wangsness, "Sublattice effects in magnetic resonance," Phys. Rev. **91**(5), 1085–1091 (1953).
[33]A. Y. Dobin and R. H. Victora, "Surface roughness induced extrinsic damping in thin magnetic films," Phys. Rev. Lett. **92**(25), 257204 (2004).
[34]E. Martínez, V. Raposo, and Ó. Alejos, "Current-driven domain wall dynamics in ferrimagnets: Micromagnetic approach and collective coordinates model," J. Magn. Magn. Mater. **491**, 165545 (2019).
[35]Y. Quessab, J. W. Xu, C. T. Ma, *et al.*, "Tuning interfacial Dzyaloshinskii-Moriya interactions in thin amorphous ferrimagnetic alloys," Sci. Rep. **10**, 7447 (2020).
[36]J. Cho, N.-H. Kim, S. Lee, J.-S. Kim, R. Lavrijsen, A. Solignac, Y. Yin, D.-S. Han, N. J. J. van Hoof, H. J. M. Swagten, B. Koopmans, and C.-Y. You, "Thickness dependence of the interfacial Dzyaloshinskii–Moriya interaction in inversion symmetry broken systems," Nat. Commun. **6**(1), 7635 (2015).
[37]A. Hrabec, N. A. Porter, A. Wells, M. J. Benitez, G. Burnell, S. McVitie, D. McGrouther, T. A. Moore, and C. H. Marrows, "Measuring and tailoring the Dzyaloshinskii-Moriya interaction in perpendicularly magnetized thin films," Phys. Rev. B **90**(2), 020402 (2014).
[38]A. Soumyanarayanan, N. Reyren, A. Fert, and C. Panagopoulos, "Emergent phenomena induced by spin–orbit coupling at surfaces and interfaces," Nature **539**(7630), 509–517 (2016).
[39]S. Tacchi, R. E. Troncoso, M. Ahlberg, G. Gubbiotti, M. Madami, J. Åkerman, and P. Landeros, "Interfacial Dzyaloshinskii-Moriya interaction in **CoFeB** films: Effect of the heavy-metal thickness," Phys. Rev. Lett. **118**(14), 147201 (2017).
[40]H. Yang, A. Thiaville, S. Rohart, A. Fert, and M. Chshiev, "Anatomy of Dzyaloshinskii-Moriya interaction at **Co/Pt** Interfaces," Phys. Rev. Lett. **115**(26), 267210 (2015).